Testing for Welding, Joining or Additive Manufacturing Applications

Tanju Teker, Sinan Aydın* and Serdar Osman Yılmaz

Joint performance of medium carbon steel-austenitic stainless steel double-sided TIG welds

https://doi.org/10.1515/mt-2022-0422

Abstract: AISI 1040 and AISI 304 steel plates of 10 mm were joined without pretreatment by double-sided TIG arc welding (DSAW). Joints were manufactured by using welding currents of 420, 440, and 460 A. The microstructural variations in the interface of the weld samples were defined by optical microscopy, scanning electron microscopy, energy dispersive spectroscopy and microhardness analysis. V-notch impact and tensile tests were done to detect the weld strength of the weld samples. In DSAW welding of different steels, a full penetration joint was achieved without opening the weld edge. The current intensity had a major effect on the symmetrical and hourglass shape in welds. Welding at 460 (A) showed acceptable joint quality. Tensile and impact energy quantities of welded joints had significant ratios. Fractures in the weld metal of the samples were ductile mode.

Keywords: AISI 1040; AISI 304; DSAW; impact test; TIG.

1 Introduction

Stainless steel (SS) has an important position in the field of engineering due to high corrosion resistance and formability properties. AISI 304 type (SS) is widely used because of high temperature resistance and environmental friendliness. AISI 316 type austenite (SS) with molybdenum level of 2 wt% has excellent corrosion and high temperature behavior. AISI 309 and AISI 310 SS with a chromium level of 23–25 wt% are used for high temperature practices. The share of austenitic stainless steels in total (SS) production is 70%, which shows that the most commonly used stainless steel type is AISI 304 austenite SS. It has the following properties: 1: Excellent corrosion resistance, 2: Excellent weldability, 3: The ability to easily shaped due to its ductility, 4: Hygienic, easy to clean and maintain, 5: Good mechanical properties at high temperatures, and 6: Excellent mechanical properties at low temperatures [1, 2]. The mechanical strength of AISI 1040 steel has average values. For this reason, this type of steel, which is preferred in most machine parts, is known as carbon steels. Cracks and fractures may occur during welding because the high carbon content of the structure causes excessive hardening in the weld zone. It is emerging as the necessity of combining materials with properties different from each other, due to increases in material types of materials used in welding sector, the necessity of variation alloy joints in places where different properties are required and especially the growing importance of economic factors in recent years [3, 4]. The welding of dissimilar alloys is more difficult than the welding of similar alloys because of the diversities in the physical, strength and metallurgical status of the materials to be welded. Various weld joints are widely applied in different areas, including nuclear, power generation, chemical, petrochemical, and other sectors. Negative impacts, for example, grain boundary corrosion, delta ferrite phase, and sigma phase taking place at the weld interface have a major impact on decreasing the characteristics of the joints. Thus, for the purpose of minimizing the above-mentioned problems, it is required to develop new methods and processes [5–7].

In the TIG welding, the heat energy required for welding is provided by the tungsten electrode and workpiece, and shielding gas is used to protect the welding area from the adverse effects of the air. The TIG welding method is easy to use by the welded, is very similar to the gas fusion welding in principle, and has a very wide application area. In some cases, it can be performed without using additional welding metal, since the inconsumable electrode is used in this method. However, if necessary, additional welding metal can be used like in gas

***Corresponding author: Sinan Aydın**, Faculty of Technology, Department of Mechatronics Engineering, Sivas Cumhuriyet University, 58140, Sivas, Türkiye, E-mail: sinancan@cumhuriyet.edu.tr. https://orcid.org/0000-0003-2285-0906

Tanju Teker, Faculty of Technology, Department of Manufacturing Engineering, Sivas Cumhuriyet University, Sivas, 58140, Türkiye

Serdar Osman Yılmaz, Faculty of Engineering, Department of Mechanical Engineering, Tekirdag Namik Kemal University, 59160, Corlu, Tekirdag, Türkiye

welding method. This welding method is becoming more and more popular due to the fact that it provides a great convenience to the welder in the extraction of the root passes and repair works [8, 9]. Chen et al. [10] explained the effect of process terms on the microstructure and mechanical properties of 5A06 aluminum alloy joined with double-side laser-TIG weld. The weld cross-sectional shape has close relation to the mechanical properties and microstructure.

In this study, 10 mm thick medium carbon steel-austenitic stainless steel was joined without pretreatment by TIG-DSAW. The hour glass shape formation, microstructure and mechanical properties in the joints were observed experimentally.

2 Experimental approach

Medium carbon steel–austenitic (SS) couples of 130 × 100 × 10 mm were welded by TIG-DSAW process. Chemical compositions of AISI 1040-AISI 304 steel couples used in experimental studies were given in Table 1. Welding operations were performed by Ge-KA-Mak TIG welding machine. Test studies were carried out by using welding parameters in Table 2. Argon gas was selected as a shielding gas in weld.

The surface of the prepared test samples was ground with 80–1200 mesh SiC abrasive paper in order to see the microstructure changes appeared in the joint zones of the welded samples. The ground samples were polished with 3 μm diamond paste. AISI 1040 steel sides were etched with a mixture of 98 wt% ethylalcohol +2 wt%HNO_3 at 3–5 s. AISI 304 steel sides were etched as 3 V electrolytic with 50 wt%HNO_3 and 50 wt% alcohol at 30 s. Afterwards, microstructural changes of the weld zones were observed by LEICA DM750 optical microscope (OM) device, scanning electron microscope (SEM) (Make: ZEISS, Japan; Model: EVO). X-ray diffraction (XRD, Model: Rigaku) patterns were described by X-ray diffractometer with a CuKα (λ = 1.5406 Å), voltage of 40 kV and 40 mA. Vickers microhardness were measured under 100 g loads by QNESS Q10 model machine. Notch impact test was carried out by JB-300S notch impact tester with a 300 J hammer. Tensile test samples which were prepared in accordance with ASTM-E8 standard were performed by pulling speed 5 mm min^{-1} using a Shimadzu device with a 50 kN. The schematic images of tensile and impact test samples are presented in Figure 1. The fracture morphology of test samples was detected by using SEM.

Table 2: Process parameters of double-sided TIG welding.

Sample no	Current intensity (A)	Shielding gas flow rate (l min^{-1})	Weld speed (m min^{-1})	Electrode diameter (mm)
*S*1	420	10	0.01	2.1
*S*2	440	10	0.01	2.1
*S*3	460	10	0.01	2.1

3 Results and discussion

3.1 Macro and microstructural evaluations

In Figure 2, the surface and interface macro photographs of test samples are given respectively. Test samples were

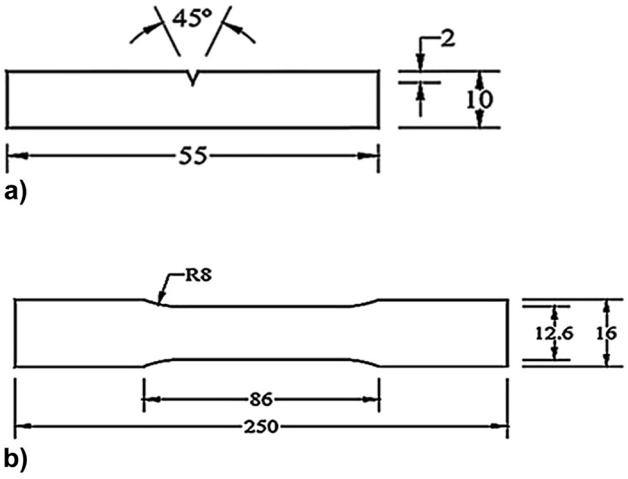

Figure 1: Schematic images of a) impact and b) tensile samples.

Table 1: Chemical contents of steels used in tests (wt%).

	Chemical contents (wt%)								
Steels	**Fe**	**C**	**Cr**	**Si**	**Ni**	**P**	**S**	**Cu**	**Mn**
AISI 1040	Bal.	0.393	–	0.156	–	0.032	0.021	0.325	0.656
AISI 304	Bal.	0.066	18.180	0.4720	8.102	0.037	0.005	0.344	1.560

successfully joined by TIG-DSAW. If the heat input remains in a narrow field during welding, the solidification of the weld will occur in a narrower field and as a result, the heat affected zone (HAZ) will be narrowed [11]. Due to the narrowing of the geometry of weld seam and the HAZ, the sensitivity of hot cracking is reduced in stainless steels and the grain size remains finer. At the same time, as the energy density of heat input is focused on a narrow area, residual stresses in the weld zone also decrease [12]. These negativities were minimized since in the TIG method; both the heat input and the depth/width rate can be easily controlled. The HAZ and the weld seam width expanded depending on the increased welding current intensity due to the increase of the energy input. In addition, there was an increase in penetration depth due to the increased current intensity. It was seen in the welds produced by TIG-DSAW that the melt metal profiles formed at the weld interface of all three samples were approximately symmetrical and hourglass shaped. There were significant differences in the hourglass profile dimensions for all three samples depending on the applied current intensity. Based on the increase in the energy degree of the heat source, a higher weld depth to bead width rate takes a significant place in the rate of energy concentration in the course of TIG process [13, 14].

Optical micrographs of *S*3 Sample are given in Figure 3, and SEM photos of welding interfaces of *S*3 Sample are shown in Figure 4. It was found that depending on the increase of the heat input, the grain coarsening significantly occurred towards the base metal from the transition zone of all three samples. The solidification of the weld zone was located towards the weld center line and the grains were oriented in the direction of heat flow. As it progressed towards the base metal which was not affected by heat, these complex and coarse regions appeared to become more homogeneous and finer structure region. In the coarse-grained zone, the formation of pinewood martensite and carbide was evidently obvious. It was considered that high values reached in the microhardness distribution of these zones. The welding process of steels, that are not similar, is usually more difficult when compared to the welding of similar steels due to different thermal expansion coefficients and chemical compositions of materials that are not similar. Therefore, the diffusion of the carbon element from higher carbon content to comparatively lower carbon content takes place [15].

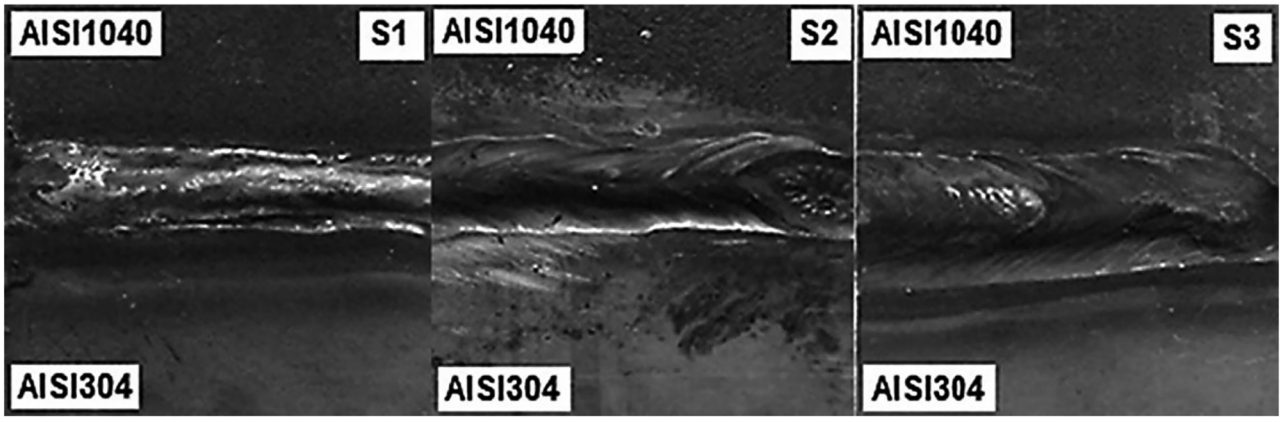

Figure 2: Appearance and geometric shape of *S*1, *S*2, and *S*3 weld joints, a) face and b) interface macro photographs.

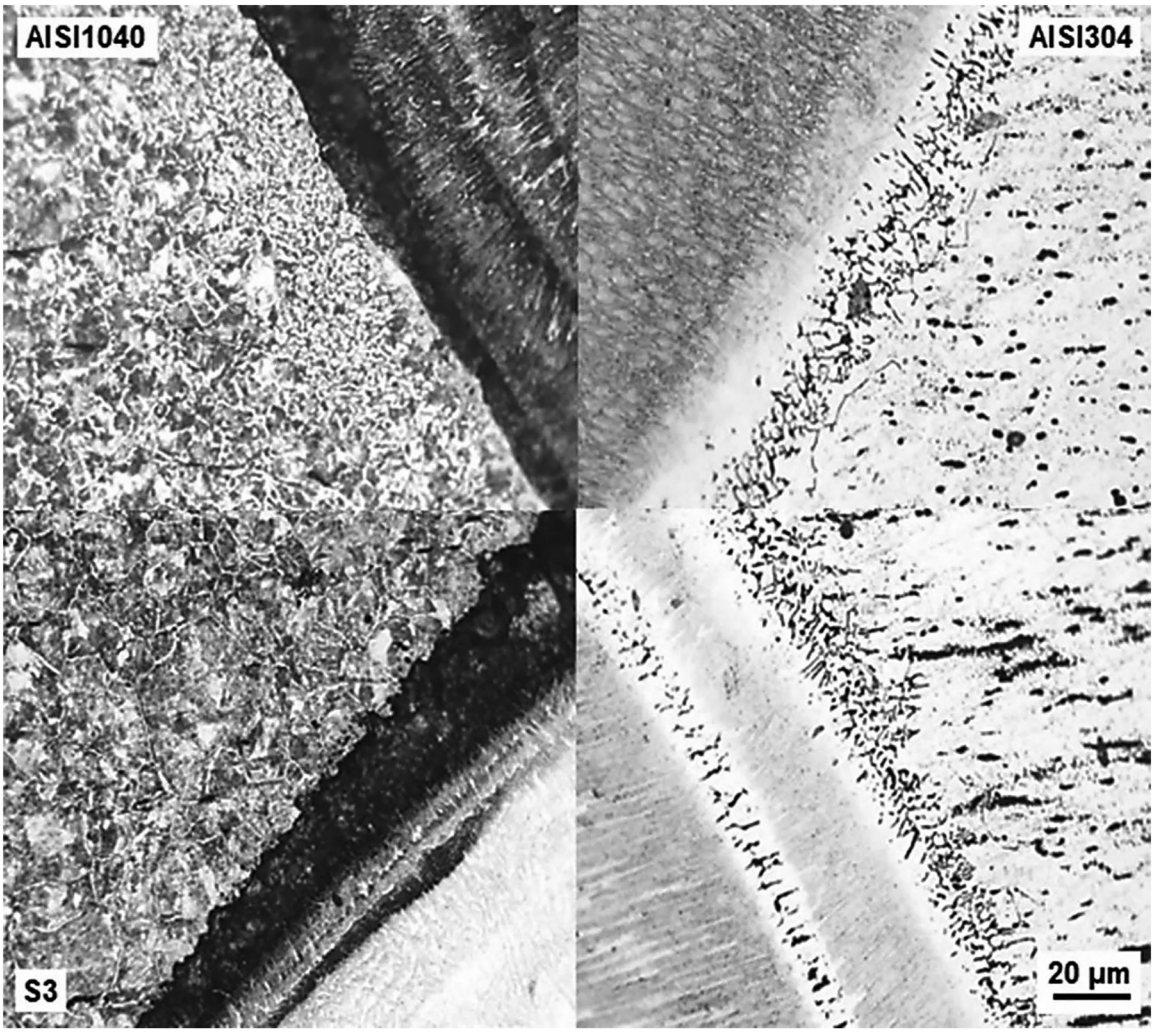

Figure 3: The interface optical micrographs of *S*3 sample.

Ferrite and small amounts of pearlite grains are presented in the AISI 1040 microstructure in Figure 3. HAZ at the AISI 1040 side is created from two various zones. At the temperature higher than AC_3 point, coarse Widmanstatten ferrite grains presented in the region near the fusion zone, and fine and recrystallized grains presented in the region near the AISI 1040 base metal. Austenite grains constituted the AISI 304 microstructure (Figure 4). HAZ at the AISI 304 side, the austenite recrystallized grains and a number of ferrites in grain boundaries formed the microstructure. The above-mentioned ferrites formed at a high temperature remain in the grain boundaries until room temperature was reached. The cooling rate in weld metal affected by the amount of heat input, and therefore, it had an impact on the metallurgical structure. The heat source had a higher energy density in TIG welding, and this led to a higher cooling speed. Therefore, the δ-ferrite phase could transform more incompletely to the austenite phase with the solidification of weld metal because of a higher cooling rate of TIG-DSAW. Thus, a higher rate of δ-ferrite observed in the weld metals at room temperature. A beneficial impact of a definite quantity of retained delta-ferrite in austenite (SS) weld determined on the decline in the susceptibility to hot cracking [1].

3.2 EDS analysis

EDS analysis results of S3 Sample were shown in Figure 5a and b respectively. The object one in AISI 1040 interface of S3 sample, it was formed from 36.84 wt%C, 60.39 wt%Fe, 0.57 wt%Mn, 1.41 wt%Cr, 0.37 wt%Si, 0.43 wt%Ni. The object two was consisted of 31.95 wt%C, 64.56 wt%Fe, 1.12 wt%Cr,

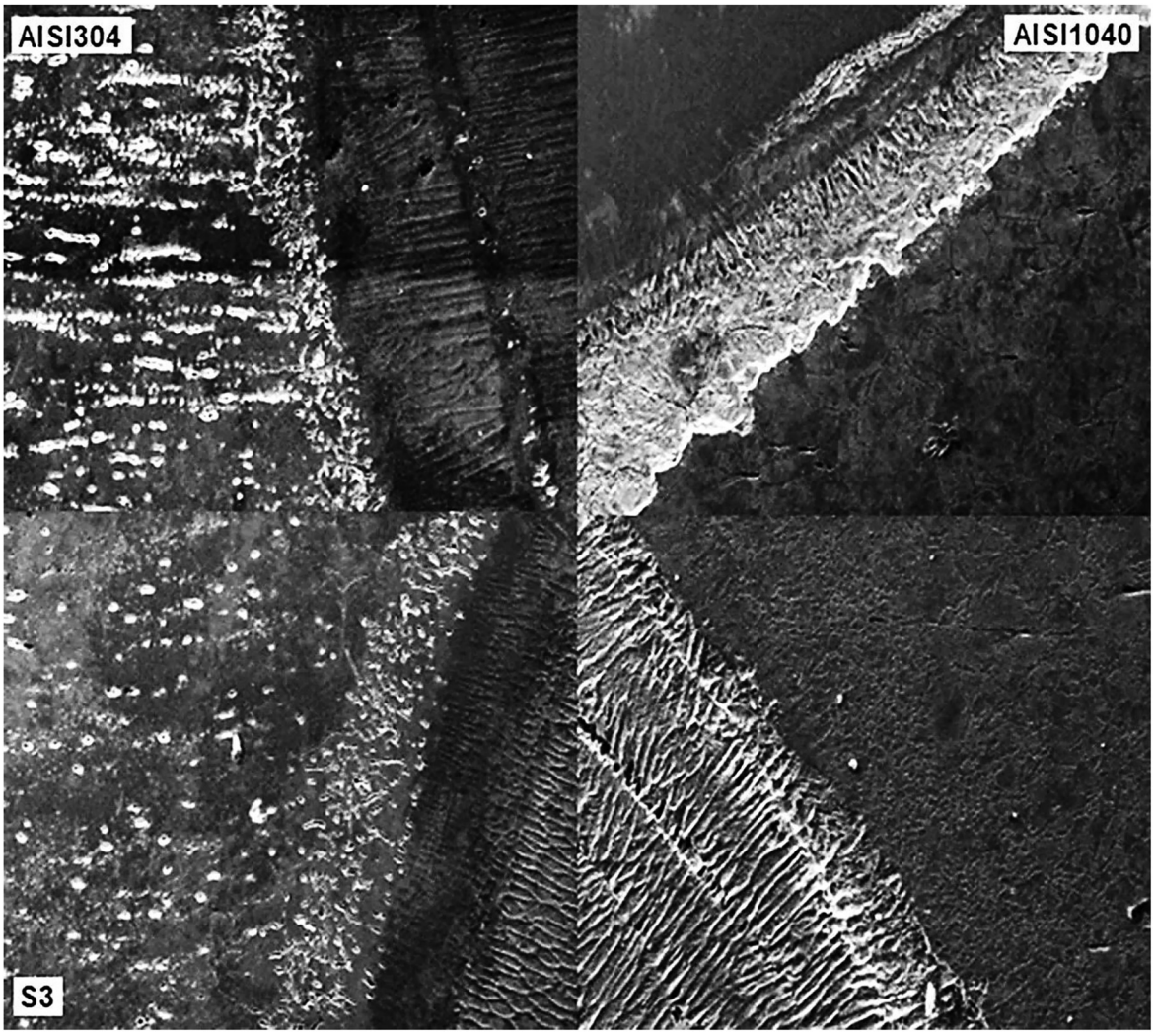

Figure 4: SEM photograph of the weld interfaces of *S*3 sample.

0.52 wt%Mn, 0.52 wt%Ni, 0.34 wt%Si (Figure 5a). The object one in AISI 304 interface of *S*3 sample was formed from 0.94 wt%Mn, 78.45 wt%Fe, 7.63 wt%Cr, 0.48 wt%Si, 7.71 wt% C and 4.83 wt%Ni. The object two was consisted of 9.18 wt%C, 65.56 wt%Fe, 1.72 wt%Cr, 0.33 wt%Mn, 7.31 wt%Ni, 0.63 wt%Si (Figure 5b). Diffusion of C and Fe elements increased from AISI 1040 steel to the weld pool. The carbon element diffused from AISI 1040 side to AISI 304 side, and chromium element diffused from AISI 304 side to AISI 1040 side. X-RD analysis of the weld zone of *S*3 Sample is given in Figure 6. Fe, $Cr_{23}C_6$, and dense Cr_7C_3 carbide formation occurred in the weld zone. M_7C_3 carbides usually formed in the form of Cr_7C_3 and inner particles and were useful in the formation of individual particles within the microstructure.

3.3 Microhardness test

Microhardness graph of weld joints is presented in Figure 7. A similar hardness distribution occurred in all three. While this distribution was the maximum at the welding center, it decreased towards the parent alloy. The highest value obtained at the welding metal center was measured as *S*1 = 289, *S*2 = 294, and *S*3 = 297 HV, respectively. Although the differences between the hardness values obtained were small, it was seen that the welding performed at high current intensities had higher hardness values. The heat input was important in joining of these kinds of materials, which revealed this situation affected the hardness values of the weld metal. As a

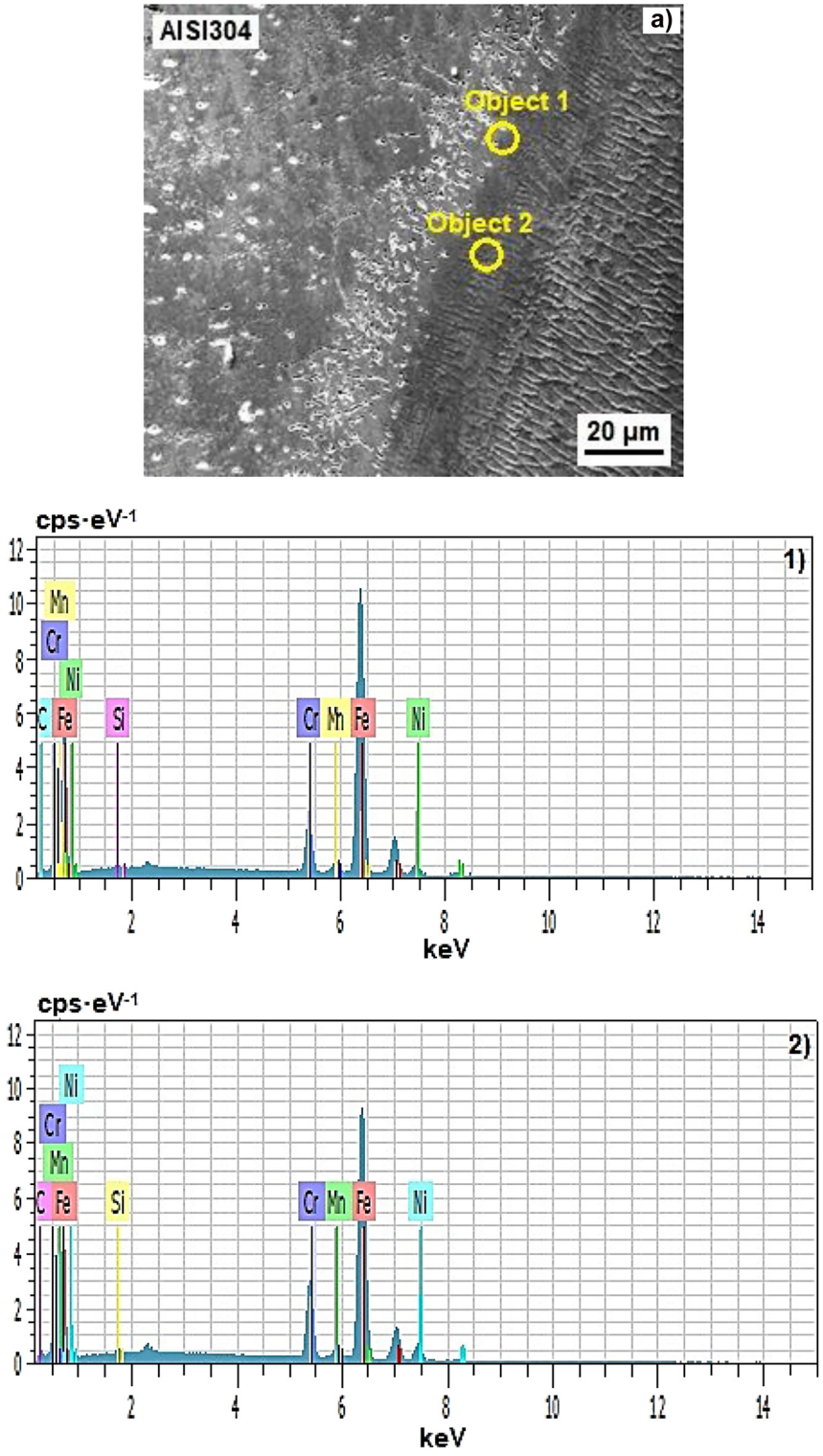

Figure 5: EDS analysis results of *S*3 sample, a) AISI 304 side and b) AISI 1040 side.

consequence of low heat input at the low current intensities, faster cooling of molten weld metal and rapid solidification, residual stresses in weld metal would result in a higher hardness value [15, 16]. The welding current intensity affected the hardness value of welded joints. The high current intensity that provided high heat input decreased the hardness value by widening the austenite area in the weld metal due to reducing the

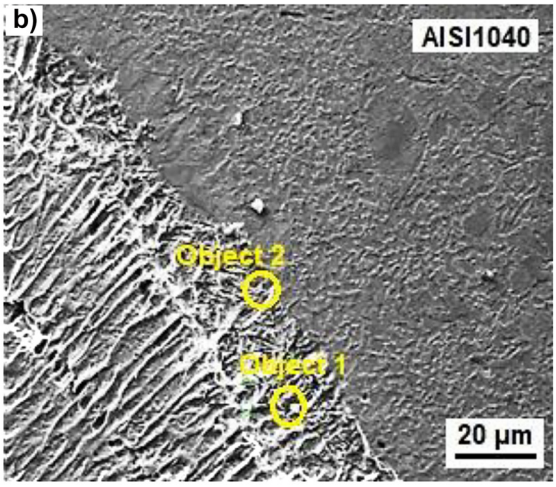

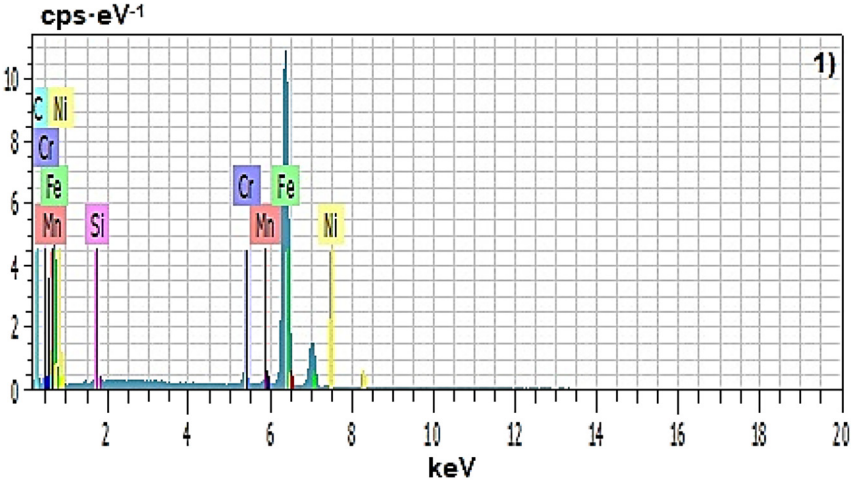

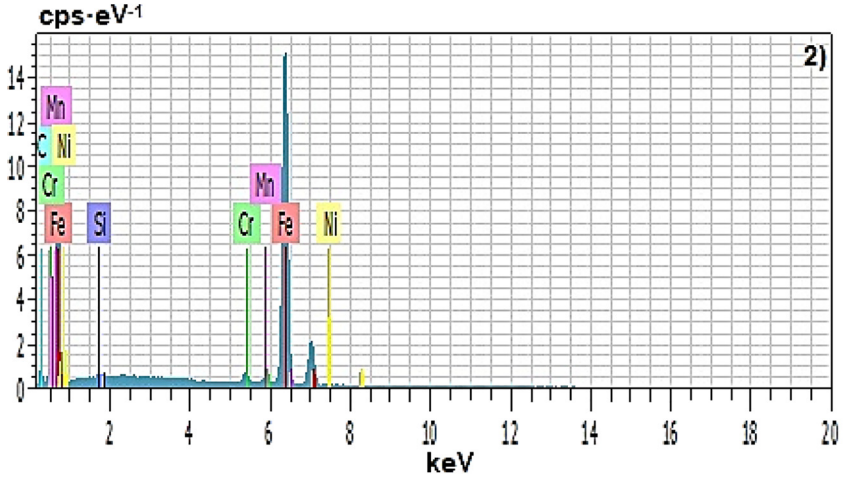

Figure 5: Continued.

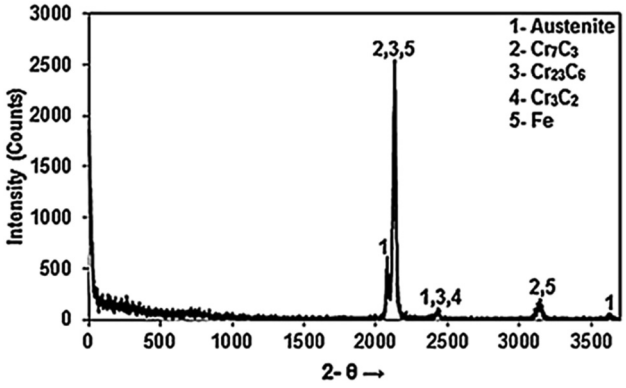

Figure 6: XRD analysis graph of *S*3 sample.

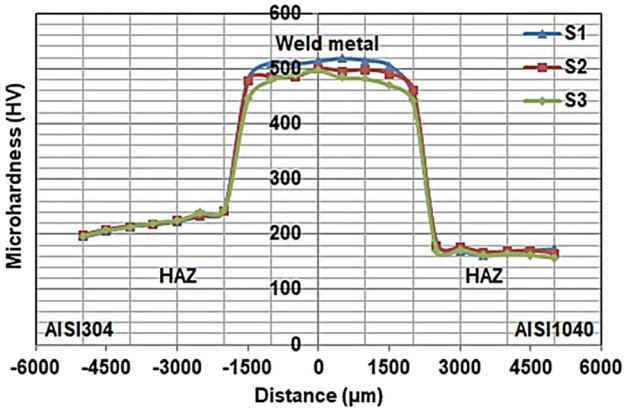

Figure 7: Microhardness graph for experimental samples.

amount of delta (δ) ferrite. A gradual small increase from 135 HV up to approximately 175 HV was determined in the hardness of the HAZ on the AISI 1040 side due to phase transformation. A change in the HAZ hardness in the AISI 304 side observed more clearly with an increase up to approximately 220 HV. The above-mentioned increase caused by the carbide precipitation, recrystallization and appear of the ferrite at the grain boundaries in the weld pool. There was a variation in the hardness of the weld zones between the hardness values of the ferritic and austenitic base metals. Hardness in the weld pool had progressively increased on traversing from the AISI 1040 to the AISI 304 side. It demonstrated that there might be a grading in composition because of dilution from two various parent metals despite the convection influences in the weld pool [17–21]. The hardness values of *S*1 and *S*2 samples containing some delta (δ) ferrite were determined to be higher when compared to the hardness value of *S*3 Sample with low eutectic ferrite content. This showed that the hardness of the welded metal in the dissimilar AISI 304/AISI 1040 joints was affected by the presence and distribution of δ-ferrite.

3.4 Tensile test

The macro photograph of the tensile test samples is displayed in Figure 8. Maximum tensile strength values were measured as *S*1 = 377.1 N mm^{-2}, *S*2 = 458.5 N mm^{-2}, and *S*3 = 561.2 N mm^{-2}. The maximum tensile strength was found in the *S*3 sample due to higher heating input. The high tensile strength and toughness values of the austenitic stainless steels combined with the TIG welding method increased depending on the geometry of the welding bath and focusing on a narrower area. During pulling, the samples were fractured from the outside of the coarse zone, since it could be shown that the austenitic weld metal, which was the coarse-grained region of the medium-carbon steel material, had a composite effect. It was clearly seen in the microstructure photos of Figure 3. Therefore, the fracture occurred out of HAZ, which was the most critical region. The failures were usually analyzed at the AISI 1040 side. A result of the experiment demonstrates that welded joints had better elongation and tensile strength when compared to TIG welding because TIG weld contains more precipitated δ-ferrite. An extremely high value of tensile strength was acquired because of similar chemical elements between the absence of inclusions and the weld metal of TIG weld and the base metal.

Figure 8: The macro photograph of the tensile test samples.

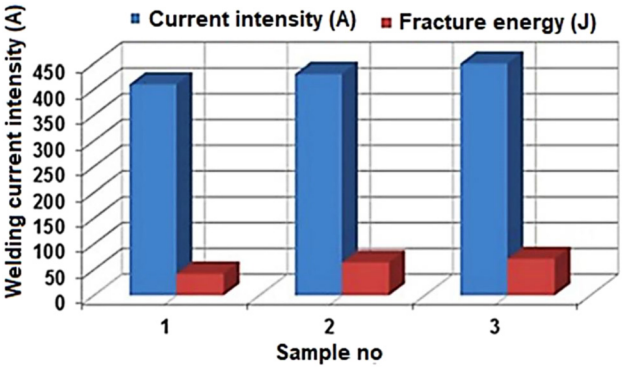

Figure 9: Notch impact test graph for *S*1, *S*2, and *S*3 samples.

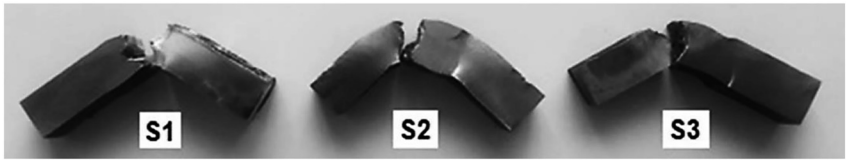

Figure 10: The macro photograph of the samples after the notch impact test.

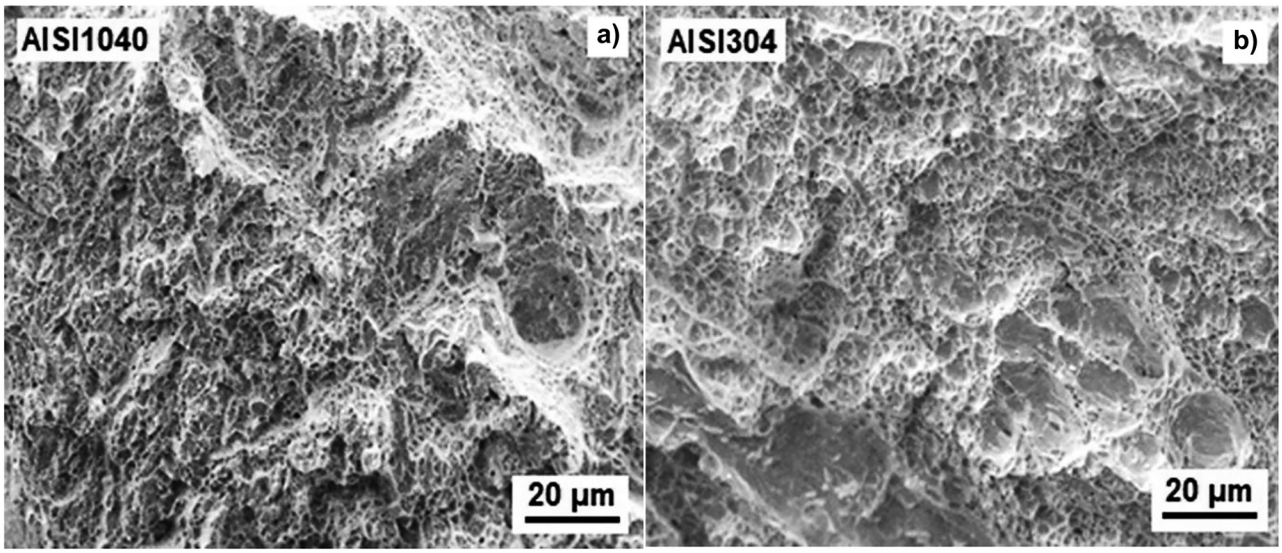

Figure 11: SEM micrographs of the fracture surface of *S*3 sample after impact test, a) AISI 1040 side and b) AISI 304 side.

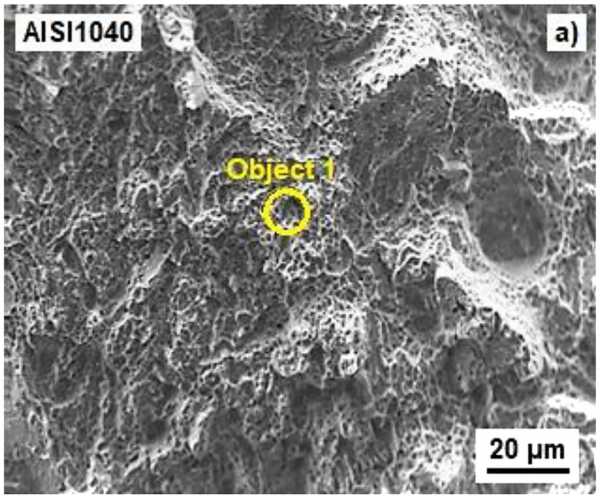

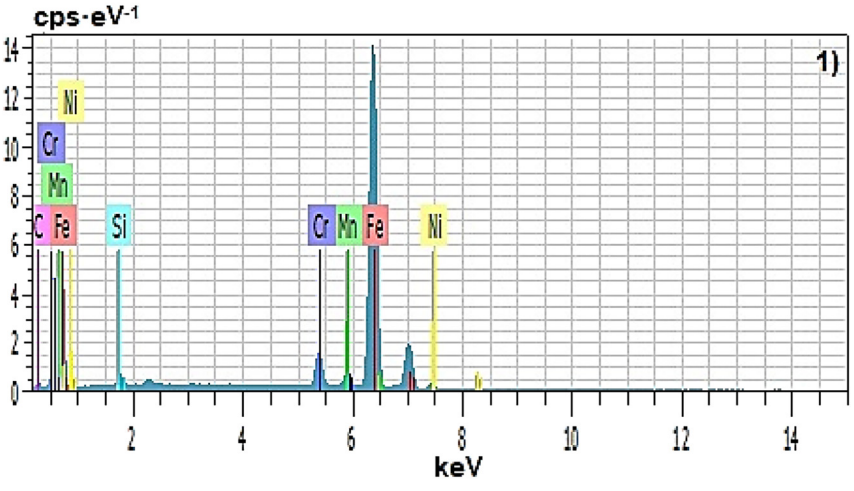

Figure 12: EDS analysis of fracture surface of *S*3 sample, a) AISI 1040 side and b) AISI 304 side.

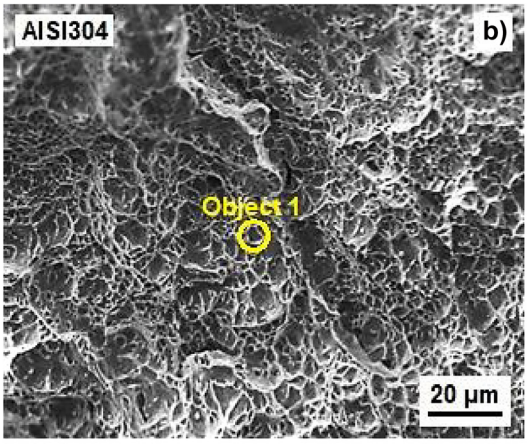

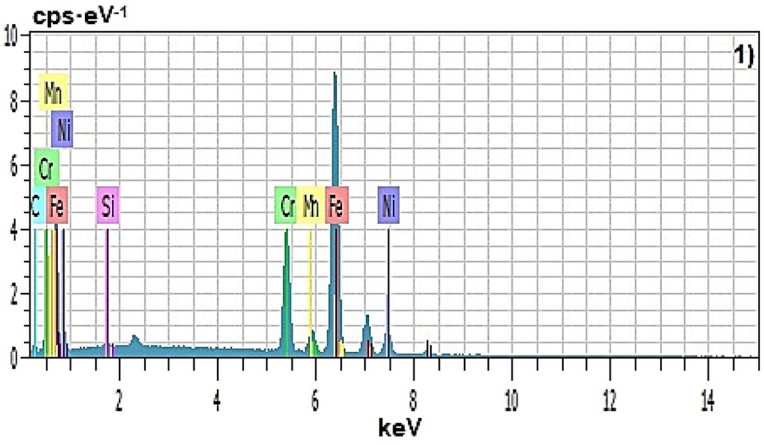

Figure 12: Continued.

3.5 Notch impact test

The notch impact test graphs of joints are shown in Figure 9, and the fracture energies were obtained as *S*1 = 41.75 J, *S*2 = 65.50 J, and *S*3 = 72.50 J. As shown in the macro photos of the samples after the notch impact test in Figure 10, plastic deformation occurred during fracture in the weld zones, which showed that the fracture was ductile. The *S*3 Sample had the highest strength with impact strength of 72.50 J. Although *S*1 and *S*2 samples had similar metallurgical properties, fracture energy values of *S*1 and *S*2 samples were recorded as 41.75 J and 65.50 J. High hardness values were reached in the coarse-grained zone of the samples under heat due to martensite formation and carbide formation [22]. Also, in these zones, coarse grains had a polygonal geometry and, in these regions, spread of cracks in the face of impact load was easy. It was thought that the joint strength had an effect on the negative direction.

3.6 Fracture surface analysis

The fractured surface photographs of the weld joints after the impact test are given in Figure 11. Fracture occurred in the weld metal of the samples were ductile mode. It was thought to be a result of the composition to have the weld metal formed by the test material used. There were fine and similar dimples on the fracture surface. EDS analysis results taken from fracture surfaces of AISI 1040 and AISI 304 sides of *S*3 sample were shown in Figure 12a and b. The point 1 in the interface of *S*3 sample, it was formed from 11.43 wt%C, 87.10 wt%Fe, 0.81 wt%Mn, 1.89 wt%Cr, 0.27 wt%Si, and 0.64 wt%Ni. The point 2 was formed from 8.14 wt%C, 77.66 wt%Fe, 1.22 wt%Cr, 0.61 wt%Mn, 0.65 wt%Ni, and 0.20 wt%Si. Elements of AISI 1040 and AISI 304 steels diffused from one metal to another with increasing welding current temperature.

4 Conclusions

The following facts were obtained.

(1) AISI 1040-AISI 304 steel plates of 10 mm were joined with the full penetration in the butt position by employing the TIG-DSAW.
(2) The current intensity had a significant effect on the symmetrical and hourglass shape in welds.
(3) The Widmanstatten ferrite and fine recrystallized grains presented in the HAZ on the AISI 1040 side. The HAZ on the AISI 304 side consisted of recrystallized grains and small ferrite at the grain boundaries.
(4) In all test parameters, hardness of the weld center was higher than HAZ and parent alloy.
(5) A decrease was determined in the impact toughness of the joining because of the increase in the delta ferrite content in the weld alloys. The highest impact energy was determined in *S*3 Sample to be 72.50 J.
(6) Tensile and impact energy quantities of joints had significant ratios.
(7) The retained δ-ferrite quantity of AISI 1040 and stainless-steel welds increased because of TIG-DSAW. Also, a decrease in hot cracking observed.

Research funding: None declared.

Author contributions: All the authors have accepted responsibility for the entire content of this submitted manuscript and approved submission.

Conflict of interest statement: No potential conflict of interest was reported by the authors.

References

[1] J. C. Lippold and D. J. Kotecki, *Welding Metallurgy and Weldability of Stainless Steel*, 5nd ed. New York, USA, John Willey & Sons, 2005.
[2] J. Wang, M. Lu, L. Zhang, W. Chang, L. Xu, and L. Hu, "Effect of welding process on the microstructure and properties of dissimilar weld joints between low alloy steel and duplex stainless steel," *Int. J. Miner. Metall. Mater.*, vol. 19, no. 6, pp. 518–524, 2012, https://doi.org/10.1007/s12613-012-0589-z.
[3] P. Sedek, J. Brozda, L. Wang, and P. J. Withers, "Residual stress relief in MAG welded joints of dissimilar steels," *Int. J. Pres. Ves. Pip.*, vol. 80, no. 10, pp. 705–713, 2003, https://doi.org/10.1016/j.ijpvp.2003.08.004.
[4] S. Missori and A. Sili, "Austenitic ferritic transition joints welded by buttering technique," in *Applications of Stainless Steels*, vol. 2, Stockholm, Sweden, Jernkontoret, 1992, pp. 986–992.
[5] K. Laha, K. S. Chandravathi, P. Parameswaran, S. Goyal, and M. D. Mathew, "A comparison of creep rupture strength of ferritic/austenitic dissimilar weld joints of different grades of Cr-Mo ferritic steels," *Metall. Mater. Trans. A*, vol. 43, no. 4, pp. 1174–1186, 2012, https://doi.org/10.1007/s11661-011-0957-8.
[6] V. V. Satyanarayana, G. M. Reddy, and T. Mohandas, "Dissimilar metal friction welding of austenitic-ferritic stainless steels," *J. Mater. Process. Technol.*, vol. 160, no. 2, pp. 128–137, 2005, https://doi.org/10.1016/j.jmatprotec.2004.05.017.
[7] Y. C. Lin and P. Y. Chen, "Effect of nitrogen content and retained ferrite on residual stress in austenitic stainless-steel weldments," *Mater. Sci. Eng., A*, vol. 307, nos. 1–2, pp. 165–171, 2001, https://doi.org/10.1016/S0921-5093(00)01821-9.
[8] C. Jang, P. Y. Cho, M. Kim, S. J. Oh, and J. Si Yang, "Effects of microstructure and residual stress on fatigue crack growth of stainless-steel narrow gap welds," *Mater. Des.*, vol. 31, no. 4, pp. 1862–1870, 2010. https://doi.org/10.1016/j.matdes.2009.10.062.
[9] C. C. Hsieh and W. Wu, "Phase transformation of $\delta \rightarrow \sigma$ in multipass heat-affected and fusion zones of dissimilar stainless steels," *Met. Mater. Int.*, vol. 17, no. 3, pp. 375–381, 2011, https://doi.org/10.1007/s12540-011-0612-3.
[10] Y. B. Chen, Y. G. Miao, L. Q. Li, and L. Wu, "Joint performance of laser-TIG double-side welded 5A06 aluminum alloy," *Trans. Nonferrous Metals Soc. China*, vol. 19, no. 1, pp. 26–31, 2009, https://doi.org/10.1016/S1003-6326(08)60223-X.
[11] M. Mukherjeey and T. K. Pal, "Influence of heat input on martensite formation and impact property of ferritic-austenitic dissimilar weld metals," *J. Mater. Sci. Technol.*, vol. 28, no. 4, pp. 343–352, 2012, https://doi.org/10.1016/S1005-0302(12)60066-8.
[12] T. Teker, "Effect of melt-in and key-hole modes on the structure and mechanical properties of AISI 430 steel welded using plasma transfer arc welding," *Phys. Met. Metallogr.*, vol. 119, no. 7, pp. 669–677, 2018. https://doi.org/10.1134/S0031918X18070116.
[13] T. Teker and D. Gençdoğan, "Mechanical performance and weldability of HARDOX 450/AISI 430 grade joined by TIG double sided arc welding," *Mater. Test.*, vol. 64, no. 11, pp. 1606–1613, 2022, https://doi.org/10.1515/mt-2022-0090.
[14] S. Wang, Q. Ma, and Y. Li, "Characterization of microstructure, mechanical properties and corrosion resistance of dissimilar welded joint between 2205 duplex stainless steel and 16MnR," *Mater. Des.*, vol. 32, no. 2, pp. 831–837, 2011, https://doi.org/10.1016/j.matdes.2010.07.012.
[15] K. H. Tseng and C. P. Chou, "Effect of pulsed gas tungsten arc welding on angular distortion in austenitic stainless steel weldments," *Sci. Technol. Weld. Join.*, vol. 6, no. 3, pp. 149–153, 2001, https://doi.org/10.1179/136217101101538686.
[16] K. H. Tseng and C. P. Chou, "The Effect of pulsed GTA welding on the residual stress of a stainless steel weldment," *J. Mater. Process. Technol.*, vol. 123, no. 3, pp. 346–353, 2002, https://doi.org/10.1016/S0924-0136(02)00004-3.
[17] T. Teker and N. Özdemir, "The effect of nozzle orifice diameter on penetration depth and mechanical properties of AISI 430/AISI 1040 dissimilar steel joined by keyhole PTA welding process," *Kovove Mater. Met. Mater.*, vol. 51, no. 4, pp. 241–249, 2013, https://doi.org/10.4149/km-2013-4-241.
[18] E. Ranjbarnodeh, S. Serajzadeh, A. H. Kokabi, S. Hanke, and A. Fischer, "Finite element modeling of the effect of heat input on residual stresses in dissimilar joints," *Int. J. Adv. Manuf. Technol.*, vol. 55, nos. 5–8, pp. 649–656, 2011, https://doi.org/10.1007/s00170-010-3095-3.
[19] S. W. Shyu, H. Y. Huang, K. H. Tseng, and C. P. Chou, "Study of the performance of stainless steel," *J. Mater. Eng. Perform.*, vol. 17, no. 2, pp. 193–201, 2008, https://doi.org/10.1007/s11665-007-9139-7.
[20] M. H. Chen and C. P. Chou, "Effect of thermal cycles on ferrite content of austenitic stainless steel," *Sci. Technol. Weld. Join.*, vol. 4, no. 1, pp. 58–62, 1999, https://doi.org/10.1179/stw.1999.4.1.58.

[21] Y. Fang, Z. Liu, S. Cui, Y. Zhang, J. Qiu, and Z. Luo, "Improving Q345 weld microstructure and mechanical properties with high frequency current arc in keyhole mode TIG welding," *J. Mater. Process. Technol.*, vol. 250, pp. 280–288, 2017, https://doi.org/10.1016/j.jmatprotec.2017.07.026.
[22] T. Teker and A. Güneş, "Microstructure and mechanical characteristics of AISI 304/DUROSTAT 500 steel double-side TIG welds," Mater. Test., vol. 64, no. 8, pp. 1162–1171, 2022, https://doi.org/10.1515/mt-2022-0033.

The authors of this contribution

Tanju Teker
Prof. Dr. Tanju Teker, born in Sivas, works in University of Sivas Cumhuriyet, Faculty of Technology, Department of Manufacturing Engineering, Sivas, Turkey. He graduated in Metallurgy Education from Gazi University, Ankara, Turkey, in 1997. He received his MSc and Ph. D degrees from Firat University, Elazig, Turkey, in 2004 and 2010, respectively. His research interests metal coating techniques, casting, fusion, and welding solid-state welding methods.

Sinan Aydın
Dr. Sinan Aydın, born in 1975, works in the University of Sivas Cumhuriyet, Faculty of Technology, Department of Mechatronics Engineering, Sivas, Turkey. He graduated in Mechanical Engineering at Cumhuriyet University, Sivas, Turkey, in 1997. He received his MSc degree at Cumhuriyet University, Sivas, Turkey in 2001 and PhD degree at Firat University, Elazig, Turkey, in 2012. He studied solid state welding methods, nano particles and adhesive technologies

Serdar Osman Yılmaz
Prof. Dr. Serdar Osman Yılmaz, born in Elazig, works at the University of Namık Kemal, Faculty of Engineering, Department of Mechanical Engineering, Corlu, Tekirdağ, Turkey. He received his BSc from METU University, Faculty of Engineering, Metallurgy and Materials Engineering Department, Ankara, Turkey, in 1989, his MSc from the Institute of Science and Technology, Metallurgy Department in 1992 and his Ph. D from the University of Firat, Institute of Science and Technology, Metallurgy Department, Elazig, Turkey, in 1998. He studied metal coating techniques, surface modification, welding, casting, and wear.